A Multidomain Pseudospectral Formulation

for the Simulation of Elastic Wave Scattering

Steen Arnfred Nielsen

Risø National Laboratory

Optics and Fluid Dynamics Department

OFD-128, DK-4000 Roskilde, Denmark

Jan S. Hesthaven

Division of Applied Mathematics

Brown University

Box F, Providence, Rhode Island 02912, USA

Received:

Running Title: Multidomain Pseudospectral Modeling of Elastic Scattering

Abstract

In many areas of acoustical imaging, such as ultrasonic non-destructive evaluation (NDE), a realistic calculation of ultrasonic field parameters and associated elastic wave scattering requires the treatment of discontinuous, layered solids in complex geometries. These facts suggest the need for an accurate and geometrically flexible numerical approach for the simulation of the ultrasonic field, rather than reliance on semi-analytic solutions.

In this paper we present an approach for solving the elastic wave equation in discontinuous layered materials in general complex geometries. The approach, based on a direct pseudospectral solution of the time-domain elastodynamic equations consists of five steps. The first step decomposes the global computational domain into a number of subdomains adding the required geometrical flexibility to the method. Moreover, this decomposition allows for efficient parallel computations, hence decreasing the computational time. The second step in the method maps every subdomain onto the unit square using transfinite blending functions. With this curvilinear mapping the elastodynamic equations can be solved to spectral accuracy, and furthermore, complex interfaces can be approximated smoothly, thus avoiding staircasing. The third step of the method deals with the evaluation of spatial derivatives on Chebyshev-Gauss-Lobatto nodal points whithin each subdomain, by means of a pseudospectral approach, while the fourth step reconstruct a global solution from the local solutions using properties of the equations of elastodynamics. Each subdomain can be prescribed with either open, physical or stress free boundary conditions. Boundary conditions are applied by means of characteristic variables. In a final step, the global solution is advanced in time using a fourth order Runge-Kutta scheme. Several examples of elastic wave

scattering related to ultrasonic NDE are presented as evidence of the accuracy and flexibility of the proposed computational method.

PACS numbers: 43.20.Bi, 43.20.Gp, 43.20.Jr, 43.35.Zc

Corresponding Author:

Steen Arnfred Nielsen

FORCE Institute

Mechatronics and Sensor Technology

Park Allé 345, DK-2650 Brøndby, Danmark

srn@force.dk

Phone. +45 4326 7573

Fax.   +45 4326 7011

I.   INTRODUCTION

Numerical solutions of the elastic wave equation are needed to study wave propagation in complex distributions of material for which analytical solutions do not exist. Such complex distributions are, in particular, found in industrial materials and have shown to be a challenge for ultrasonic non-destructive evaluation (NDE) systems in which the main interest is the recorded transducer signals (A- and B-scans) arising due to elastic scattering from material cracks[1-2]. Much has been written on scattering of ultrasonic waves by inhomogeneities[3-4] and its effect on ultrasonic images[5-6] and quantitative NDE[7-8].

Modeling of the elastic wave equation began around 1970 with the finite difference (FD) method. Alford *et al.*[9] model acoustic scattering with a higher order scheme and Kelly *et al.*[10] show how complex interfaces can be incorporated into the simulations. These techniques handle most complex material geometries but are limited by numerical dispersion, preventing the modeling of waves propagating over large distances, as well as the inability to impose the correct conditions on the statevariables across material interfaces. In the early eighties pseudospectral (PS) methods were introduced to enable more accurate long time simulations of acoustic and elastic scattering. Kosloff *et al.*[11] and Fornberg[12] solve the acoustic wave equation using a two-dimensional Fourier PS method and conclude that it is more accurate than a FD scheme. Another early paper of interest is Ref. [13], which shows how Fourier PS methods can be applied to problems with complex interfaces. The Fourier PS method is reviewed in Refs. [14-16]. Fourier series are convenient for problems with periodic boundary conditions, but when the solutions are non-periodic, polynomial approximations are a more natural choice. Raggio[17] solves the acoustic wave equation with a Chebyshev PS scheme.

Tessmer *et al.*[18] and Kosloff *et al.*[19] apply a combined Fourier and Chebyshev method to compute wave propagation in a seismic environment with surface topography and propose a three-dimensional implementation[20]. Moreover, essentially one-dimensional multidomain formulations have been proposed for irregular domains[21-22]. In order to allow elastic waves to pass out from the domain without reflections, absorbing boundary conditions for elastic waves have been used in many variations. See for example Refs. [23-27]. Moreover, mappings may be used to enhance the accuracy of the Chebyshev PS method[28]. More recently, Chebyshev spectral multidomain techniques have become a standard tool in fluid dynamics[29-30], and is emerging as such in computational electromagnetics[31-32]. A more comprehensive review of spectral methods for hyperbolic problems can be found in Refs. [33-34].

In this paper, we present an approach for solving the elastic wave problem in general complex distributions of materials using a pseudospectral multidomain formulation. The pseudospectral elastodynamic (PSE) method computes a direct solution to the elastodynamic equations in the time domain. In this approach, the general computational domain is split into a number of smaller subdomains, each chosen such that they can be smoothly mapped onto a unit square. This decomposition is performed in a fully bodyconforming way to avoid problems with staircase approximations and the associated errors. This enables the representation of general material distributions and allows for the construction of a pseudospectral approximation of derivatives within each of the smaller domain and hence an accurate updating of the local fields. To recover the global solution from the many local solutions a characteristic decomposition in homogeneous regions of the computational domain is used while physical boundary and interface conditions are imposed where required.

The elastic equations are advanced in time using a 4th order accurate explicit Runge-Kutta method and an absorbing matched layer is used to truncate the computational domain in an approximately reflectionless manner.

In the following section the governing elastodynamic equations are introduced on vector form and scattering by elastic waves are discussed. In section III, the features of the multidomain Chebyshev scheme are described. Section IV gives examples of wave propagating in elastic half-spaces illustrated by snapshots of the velocity field at particular times and serves as an evaluation of the scheme while Section V contains a few concluding remarks.

II. FORMULATION

This section contains two parts. In part A, the governing elastodynamic equations are introduced on vector form and, in part B, elements of elastic wave scattering are reviewed.

A. Elastodynamic Equations

The governing elastodynamic wave equation for a two-dimensional isotropic solid are based on a solution of the equations of conservation of momentum combined with the stress-strain relations for a linear elastic solid undergoing infinitesimal deformations[35]. The elastodynamic equations are given by a system of two coupled wave equations, as[36-37]

$$\rho\left(f_x + \frac{\partial^2 u_x}{\partial t^2}\right) = \frac{\partial \sigma_{xx}}{\partial x} + \frac{\partial \sigma_{xz}}{\partial z},$$

$$\rho\left(f_z + \frac{\partial^2 u_z}{\partial t^2}\right) = \frac{\partial \sigma_{xz}}{\partial x} + \frac{\partial \sigma_{zz}}{\partial z},$$

$$\sigma_{xx} = (\lambda + 2\mu)\frac{\partial u_x}{\partial x} + \lambda\frac{\partial u_z}{\partial z}, \tag{1}$$

$$\sigma_{zz} = (\lambda + 2\mu)\frac{\partial u_z}{\partial z} + \lambda\frac{\partial u_x}{\partial x},$$

$$\sigma_{xz} = \mu\left(\frac{\partial u_x}{\partial z} + \frac{\partial u_z}{\partial x}\right).$$

In this system of equations $\boldsymbol{u}=(u_x, u_z)^{\mathrm{T}}$ is the displacement vector, $\boldsymbol{\sigma}=(\sigma_{xx}, \sigma_{zz}, \sigma_{xz})$ represents the symmetric stress tensor and (x,z) are the Cartesian coordinates. $\lambda(x,z)$ and $\mu(x,z)$ are the Lamé constants (i.e. rigidity and shear modulus, respectively, for fluids: $\mu=0$), t is the time and $\rho(x,z)$ is the mass density. The body force is given as $\boldsymbol{f}=(f_x, f_z)$ and represents the applied source.

The elastodynamic equations in (1) can be recast into a hyperbolic velocity-stress system of first order in time. This formulation consists of five coupled first-order partial differential equations

$$\rho\frac{\partial v_x}{\partial t} = \frac{\partial \sigma_{xx}}{\partial x} + \frac{\partial \sigma_{xz}}{\partial z} - \rho f_x,$$

$$\rho\frac{\partial v_z}{\partial t} = \frac{\partial \sigma_{xz}}{\partial x} + \frac{\partial \sigma_{zz}}{\partial z} - \rho f_z,$$

$$\frac{\partial \sigma_{xx}}{\partial t} = (\lambda + 2\mu)\frac{\partial v_x}{\partial x} + \lambda\frac{\partial v_z}{\partial z}, \tag{2}$$

$$\frac{\partial \sigma_{zz}}{\partial t} = (\lambda + 2\mu)\frac{\partial v_z}{\partial z} + \lambda\frac{\partial v_x}{\partial x},$$

$$\frac{\partial \sigma_{xz}}{\partial t} = \mu\left(\frac{\partial v_x}{\partial z} + \frac{\partial v_z}{\partial x}\right).$$

Here, v is the particle velocity vector related to u as $v = \dfrac{\partial u}{\partial t}$.

Introducing $q = \left[v_x, v_z, \sigma_{xx}, \sigma_{zz}, \sigma_{xz}\right]^T$ as the state vector, describing the state of the system, Eq. (2) takes the simple vector form

$$\frac{\partial q}{\partial t} = A_1 \frac{\partial q}{\partial x} + A_2 \frac{\partial q}{\partial z} + S \tag{3}$$

where A_1 and A_2 are matrices containing the isotropic material parameters

$$A_1 = \begin{pmatrix} 0 & 0 & \rho^{-1} & 0 & 0 \\ 0 & 0 & 0 & 0 & \rho^{-1} \\ \lambda + 2\mu & 0 & 0 & 0 & 0 \\ \lambda & 0 & 0 & 0 & 0 \\ 0 & \mu & 0 & 0 & 0 \end{pmatrix}, \quad A_2 = \begin{pmatrix} 0 & 0 & 0 & 0 & \rho^{-1} \\ 0 & 0 & 0 & \rho^{-1} & 0 \\ 0 & \lambda & 0 & 0 & 0 \\ 0 & \lambda + 2\mu & 0 & 0 & 0 \\ \mu & 0 & 0 & 0 & 0 \end{pmatrix}, \tag{4}$$

and the body forces are given as $S = \left[-\rho f_x, -\rho f_z, 0, 0, 0\right]^T$.

B. Scattering by Elastic Waves

In general, scattering originates from waves of different type impinging on complex interfaces. The most significant waves are compressional waves and vertically polarized shear waves (denoted P-waves and S-waves, respectively) with wave speeds

$$C_p = \sqrt{\frac{(\lambda + 2\mu)}{\rho}}, \quad C_s = \sqrt{\frac{\mu}{\rho}}. \qquad (5)$$

The ratio between the velocities of the two wave types is

$$\frac{C_s}{C_p} = \sqrt{\frac{1-2\nu}{2(1-\nu)}}, \qquad (6)$$

where the Poisson ratio, ν, being given as

$$\nu = \frac{1}{2}\left[\frac{1-2C_s^2/C_p^2}{1-C_s^2/C_p^2}\right]. \qquad (7)$$

For industrial solids related to ultrasonic NDE, it is often assumed that the Poisson ratio is between 0-0.5. In ferritic steel, for example, the Poisson ratio is around 0.29 and thus $C_s/C_p \approx 0.5$. This means, that the compressional velocity is about 50 percent larger than the shear wave velocity. Since the PSE approach is based on the elastodynamic wave equations without physical approximations, the approach accounts not only for direct P- and S-waves, reflected waves (PP, SS), and multiply reflected waves (PPP, SSS), but also for converted reflected waves (PS, SP), refracted waves (PR, SR), diffracted waves (PD, SD), head waves (H), and interfacial waves. Among the latter are for example Rayleigh (R) and Stoneley (St) waves. Rayleigh waves travel along the surface of the solid while Stoneley waves travel

along internal interfaces between two elastic domains. Generally, these waves travel slower than the shear wave and decays exponentially away from the interface.

III. NUMERICAL APPROACH

The PSE-approach for solving the elastic wave equation in complex geometries containing general material properties consists of a few steps. The first step decomposes the global computational domain into a number of bodyconforming subdomains. The second step in the method maps every subdomain onto the unit square using transfinite blending functions. These two steps enable the elastodynamic equations to be evaluated using pseudospectral methods, and furthermore, complex interfaces can be approximated in a smooth bodyconforming way. The third step deals with the construction of a global solution from the local solutions as well as enforcing the correct boundary condition as being either open, physical or stress free. In the final step, the global solution is advanced in time using a fourth order Runge-Kutta scheme.

This section contains a discussion of the PSE-approach. In part A, complex geometries are incorporated using a curvilinear representation. In part B, the approximation of spatial derivatives by a Chebyshev collocation scheme is discussed, while part C addresses how local solutions are patched using characteristic variables to recover the global solution.

A. Curvilinear Formulation

To enable the representation of general distributions of materials and interfaces while maintaining a high accuracy, the global computational domain is split into a number of smaller subdomains, each chosen such that they can be smoothly mapped to a unit square. As the general blocks are curvilinear a mapping is chosen to connect the physical grid with the local computational grid as illustrated in Fig. 1. The curviliniar physical grid has the coordinates (x,z) whereas the rectangular grid has the coordinates (ξ, η) connected as

$$\xi = \xi(x, z), \qquad \eta = \eta(x, z).$$ (8)

By applying the chain rule, Eq. (3) can be written in the curvilinear representation as

$$\frac{\partial \boldsymbol{q}}{\partial t} = \boldsymbol{A}(\nabla \xi) \frac{\partial \boldsymbol{q}}{\partial \xi} + \boldsymbol{A}(\nabla \eta) \frac{\partial \boldsymbol{q}}{\partial \eta} + \boldsymbol{S}.$$ (9)

Setting $\boldsymbol{n}=(n_x, n_z)$, the matrix $\boldsymbol{A}(\mathbf{n})$ is given as

$$\boldsymbol{A}(\mathrm{n}) = \begin{pmatrix} 0 & 0 & n_x/\rho & 0 & n_z/\rho \\ 0 & 0 & 0 & n_z/\rho & n_x/\rho \\ (\lambda+2\mu)n_x & \lambda n_z & 0 & 0 & 0 \\ \lambda n_x & (\lambda+2\mu)n_z & 0 & 0 & 0 \\ \mu n_z & \mu n_x & 0 & 0 & 0 \end{pmatrix}.$$ (10)

Transfinite blending functions are used to establish a connection between the physical curvilinear grid and the auxiliary gird. A complete treatment of these functions may be found in Gordon *et al.*[38-39].

B. Pseudospectral Differentiation

In the Chebyshev method a function $q(\xi)$ is approximated by the polynomial

$$q(\xi) = \sum_{j=1}^{N} \phi_j(\xi) q(\xi_j),$$ (11)

that interpolates $q(\xi)$ at N distinct collocation points ξ_j. Due to the non-periodic nature of the problem the grid points are chosen as the Chebyshev-Gauss-Lobatto points

$$\xi_j = \cos\left(\frac{\pi(j-1)}{N-1}\right) \qquad j = 1,...,N,$$ (12)

and interpolation between the collocation points is based on the Chebyshev-Lagrange polynomials given as

$$\phi_j(\xi) = \frac{(-1)^j \left(1-\xi^2\right) T_{N-1}'(\xi)}{c_j(N-1)^2(\xi-\xi_j)},$$ (13)

where $c_1 = c_N = 2$ and $c_2 = c_3 = ... = c_{N-1} = 1$. T_{N-1} is the Chebyshev polynomial of order *N-1* defined as

$$T_{N-1}(\xi) = \cos((N-1)\cos^{-1}\xi),$$
(14)

where the computational domain is the region $\xi \in [-1,1]$.

The spatial derivative of *q(ξ)* is calculated by analytically differentiating the interpolation polynomial and the differentiation operator may then be represented by a matrix $D_{jk} = \phi'_k(\xi_j)$. Hence, the approximative derivative of *q(ξ)* at the collocation points can be found by a matrix *D* multiplying the values of *q(ξ)* at the collocation points

$$\frac{dq}{d\xi}(\xi_j) = \sum_{k=1}^{N} D_{jk} q(\xi_k),$$
(15)

where the differentiation matrix has the entries[29,34]

$$D_{jk} = \begin{cases} \frac{c_k}{c_j} \frac{(-1)^{j+k}}{c_j(\xi_k - \xi_j)} & j \neq k \\ -\frac{1}{2} \frac{\xi_k}{(1-\xi_k)^2} & j = k \neq 1, N \\ \frac{2(N-1)^2+1}{6} & j = k = 1 \\ -\frac{2(N-1)^2+1}{6} & j = k = N \end{cases}.$$
(16)

The cost of computing the derivative from the matrix multiplication is O(N^2) operations. In two dimensions, spatial derivatives are calculated using Eq. (18) and a matrix-matrix product.

C. Multidomain Formulation and boundary conditions

Once the computational domain is divided into a number of subdomains consisting of curvilinear quadrilaterals, the spatial derivatives are computed locally on each domain, and the solution to the elastodynamic equations are advanced in time with a fourth-order Runge-Kutta scheme. In order to recover a global solution from the subdomains, two strategies of interchanging internal information are employed. On boundaries between materials with different elastic constants, continuity of stress and displacement vector is required. On boundaries between materials with the same elastic constants a reconstruction based characteristic variable is employed. The boundary conditions at a stress-free surface require the stress to vanish.

In order to patch the local solutions, the characteristic variables of the matrix $A = A_1 n_x + A_2 n_z = Q \Lambda Q^{-1}$ is used. Hence, the diagonal eigenvalue matrix $\Lambda_{ii} = \lambda_i$ has the entries corresponding to the characteristic velocities $(0, C_p, -C_p, C_s, -C_s)$ and Q^{-1} with $n = |n| (\hat{n}_x, \hat{n}_z)$ is given as

$$
Q^{-1}(n) = \begin{bmatrix}
0 & 0 & \frac{-2\mu n_z^2 + \lambda(n_x^2 - n_z^2)}{\lambda+2\mu} & \frac{-2\mu n_x^2 - \lambda(n_x^2 - n_z^2)}{\lambda+2\mu} & \frac{4(\lambda+\mu)n_z n_x}{\lambda+2\mu} \\
n_x\sqrt{\frac{\rho}{\lambda+2\mu}} & n_z\sqrt{\frac{\rho}{\lambda+2\mu}} & \frac{n_x^2}{\lambda+2\mu} & \frac{n_z^2}{\lambda+2\mu} & \frac{2n_x n_z}{\lambda+2\mu} \\
-n_x\sqrt{\frac{\rho}{\lambda+2\mu}} & -n_z\sqrt{\frac{\rho}{\lambda+2\mu}} & \frac{n_x^2}{\lambda+2\mu} & \frac{n_z^2}{\lambda+2\mu} & \frac{2n_x n_z}{\lambda+2\mu} \\
-\frac{1}{2}n_z\sqrt{\rho\mu} & \frac{1}{2}n_x\sqrt{\rho\mu} & -\frac{1}{2}n_x n_z & \frac{1}{2}n_x n_z & \frac{1}{2}\left(n_x^2 - n_z^2\right) \\
\frac{1}{2}n_z\sqrt{\rho\mu} & -\frac{1}{2}n_x\sqrt{\rho\mu} & -\frac{1}{2}n_x n_z & \frac{1}{2}n_x n_z & \frac{1}{2}\left(n_x^2 - n_z^2\right)
\end{bmatrix}. \quad (17)
$$

The characteristic variables take the form

$$\boldsymbol{R} = \boldsymbol{Q}^{-1}(\boldsymbol{n})\boldsymbol{q} = \begin{bmatrix} R_1 & R_2 & R_3 & R_4 & R_5 \end{bmatrix}^T. \qquad (18)$$

Once the characteristic variables are recovered, one can exploit the signs of the corresponding eigenvalues to determine how to pass information between two neighboring elements. Indeed, based on the signs of the eigenvalues, one may observe that R_2 and R_4 will be propagating along the direction of the normal, i.e., they will leave the computational domain. Hence, they need not to be altered but will enter the neighboring element. Conversely, R_3 and R_5 will enter the current element and will need to be prescribed. This is done by passing the information from R_2 and R_4 from the neighboring element into the present one as what leaves one domain must enter the neighboring domain. Finally it may be observed that R_1 is not propagating and it is required to be continuous. Once the characteristic variables have been updated within the element as discussed above, the corrected state vector can be recovered and the patching of two elements is completed. This procedure is then repeated along every element interface at every time step to continuously recover the global solution from the many local solutions and ensure that information is propagating in accordance with the nature of the problem.

Open boundary conditions for simulating an infinite medium and avoiding non-physical reflections from the boundaries of the numerical grid is implemented using a matched absorbing layer. This layer is introduced through an absorbing term added to Eq. (9) as described in Ref. [40].

IV. NUMERICAL RESULTS

In this section numerical examples of elastic wave scattering related to ultrasonic NDE are presented. In part A, elastic scattering from a plane slit (crack) is calculated. Part B discusses elastic scattering from a two-layer elastic solid, while part C presents snapshots of scattering by an elastic cylinder.

A. Elastic Scattering from a Slit

The first example involves wave propagation in a two-dimensional homogeneous elastic half-space with a body force applied at the stress-free surface. This example is a classical modeling problem in NDE called Lamb's problem. The P- and S-wave velocities for the solid are set to 1 and $\sqrt{3}$, respectively, corresponding to a Poisson ratio of 0.25. As a first test case, the 2D pseudospectral code is compared with a 3D analytical solution. The analytical solution was found by the Cagniard-de Hoop formalism giving an analytical solution in time for Green's function. The corresponding velocity component was then derived by convoluting the Green's function with a source signal, which here was set to a pulsed raised-cosine signal. The numerical and analytical time solutions (A-scans) were compared for v_z. From Table I it can be seen that there is excellent agreement between the two solutions even for as few as 14 grid points per spatial wavelength. The global error (or infinity norm) was not improved for decreasing time step, due to the fundamental difference between the 2D and 3D solution.

In the next test case, the body force is a directional force applied at the stress free surface and representing a source transducer. In this example a Gaussian distribution for the point source was used and a time history, *s(t)* set to

$$s(t) = -\alpha \cos(2\pi(t - t_0))e^{-\beta(t-t_0)^2} , \tag{19}$$

where α, β, and t_o are constants. The current examples consider a rectangular computational domain consisting of 40 subdomains, each with 16x16 grid points, as shown in Fig. 2. The source was set on a stress free boundary, while the other sides were open (absorbing) boundaries. The vertical slit illustrates an infinitesimal thin stress free notch or crack.

Figure 3 displays elastic scattering from a vertical stress free slit due to the vertical point force. The vertical velocity component v_z is seen at different times (a) $t = 1.8$ μs, (b) $t = 4.1$ μs, and (c) $t = 5.5$ μs. Figure 3a, shows the P-, S- and R-wave just after leaving the point source at the free surface and Figs. 3b and 3c illustrate the Head (H) wave propagation. The head wave originates at the vertical slit together with the P-wave and ends at the S-wave front where it is perpendicular with the radius vector. The angle of the head wave with respect to vertical depends, as expected, on the ratio between the two velocities, i.e. the Poisson ratio, as seen in Eq. (7). Notice, that no artificial reflections are observed at the open boundaries due to the matched absorbing layer.

Figure 4 displays elastic scattering from a horizontal slit due to the vertical point force. The vertical velocity component v_z is seen at different times (a) $t = 4.1$ μs, (b) $t = 5.5$ μs, and (c) $t = 8.2$ μs. Figure 4a shows the reflected PP-wave after impinging on the horizontal stress-free

slit. In Fig. 4b, the wave develops and several wave phases are present, including the diffracted pressure wave (PD) and Rayleigh wave (R). As can be appreciated, the P-wave looses amplitude with time due to geometrical spreading, while the Rayleigh wave keeps the same amplitude since it is confined to the slit. Figure 4c shows the multiply reflected wave (PPP) due to the stress-free slit and the free surface.

The corresponding time history (A-scan) is seen in Fig. 5 for two different receiver positions on the stress-free surface. The first receiver position is identical with the transmitter (i.e. a pulse-echo transducer) and indicated with a dotted line. In this position, the initial wave pulse is followed by the PP-wave reflected from the horizontal slit. The second receiver position is illustrated in Fig. 2 and as indicated with a solid line in Fig. 5, the S-wave is proceeded by the PP-wave.

B. Scattering from a Two-Layer Elastic Solid

The second example illustrates scattering from a two-layered elastic solid. The model consists of two different elastic regions, e.g. a steel rod embedded in a lead coating with material parameters given in Table II. The calculations were performed on the same grid as used in the previous example, but with the extension of an elastic steel layer in 5 subdomains. The time interval was 19.5 ns and the total calculation time was 9.8 μs.

Figure 6 illustrates snapshots at times (a) $t = 7.4$ μs and (b) $t = 9.8$ μs of the particle velocity. It may be noticed from Fig. 6a, that the P-wave is refracted according to Snell's law within the steel rod and that the polarity of the reflected P-wave (PP) is changed. In Fig. 6b, a

diffracted P-wave (PD) is seen near the edge of the steel rod and a Stoneley (St) wave may also be identified along the interface of the two elastic solids.

C. Scattering from an Elastic Cylinder

The final example illustrates scattering by an elastic cylinder. This example is chosen because it appears frequently in the NDE community. The model consists of the same two different elastic regions as used in the previous example. The transmitting line source (i.e. transducer) is located at the stress free surface and consists of 11 point sources distributed evenly over three subdomains. The computational domain consisted of 29 subdomains, each with 20 x 20 grid points, as shown in Fig. 7. Figure 8 displays elastic scattering by an elastic cylinder due to the transducer. The velocity component is seen at different times (a) $t = 4.9$ µs and (b) $t = 7.1$ µs. Figure 8a, shows the P-wave impacting the elastic steel cylinder. The steel cylinder has a magnifying effect on the P-wave due to the faster velocity compared with the lower velocity in lead. In Fig. 8b, the Stoneley (St) wave is seen clearly propagating along the cylinder. For this calculation, the time interval was 2.37 ns and the wave propagation time was 14.2 µs. The CPU-time for each time step was about 5.1 seconds, corresponding to a total computational time of about 8 hours. The corresponding backscattered velocity profile (B-scan) was calculated from 11-point receivers distributed over the aperture of the transducer. The B-scan is seen in Fig. 9 and is usually the main component in solving the inverse problem. Here, it corresponds to a single projection.

V. CONCLUSIONS

A multidomain pseudospectral method is proposed for the simulation of scattering from complex interfaces in elastic media. The method is based on a Chebyshev pseudospectral formulation and computes a direct time-domain solution of the elastodynamic equations. Complex interfaces are resolved with a curvilinear multidomain representation and local solutions are patched using characteristic variables.

The first example demonstrate the ability of the PSE-approach to accurately compute scattering from a plane stress free slit and illustrate different wave types. The second and third example demonstrate elastic scattering from two elastic regions with a plane and cylindrical shape. Clear indications of interfacial waves caused by the elastic cylinder were observed.

ACKNOWLEDGMENTS

REFERENCES

[1] R. Ludwig and W. Lord, "A finite-element formulation for the study of ultrasonic NDT systems", *IEEE Trans. Ultrason. Ferrelec. Freq. Cont.* **35**(6), 809-820 (1988).

[2] A.S. Eriksson, J. Mattsson and A.J. Niklasson, "Modelling of ultrasonic crack detection in anisotropic materials", *NDT&E International* **33**, 441-451 (2000).

[3] P. Fellinger, R. Marklein, K.J. Langenberg and S. Klaholz, "Numerical modeling of elastic wave propagation and scattering with EFIT – elastodynamic finite integration technique", *Wave Motion* **21**, 47-66 (1995).

[4] K.J. Langenberg, P. Fellinger, R. Marklein, P. Zanger, K. Mayer and T. Kreutter, "Inverse Methods and Imaging". In: *Evaluation of Materials and Structures by Quantitative Ultrasonics* (Ed.: J. D. Achenbach), Springer-Verlag, Vienna, (1993).

[5] S.A. Nielsen, J.T. Rheinländer, K.K. Borum, and H.E. Gundtoft, "Three-dimensional ultrasonic reflection tomography of cylindrical shaped specimens". In: *European Conf. on NDT* (Ed. B. Larsen), Denmark, **3**, 2458-2465, (1998).

6   S.A. Nielsen and L. Bjørnø, "Bistatic circular array imaging with gated ultrasonic signals". In: *Acoustical Imaging* (Eds.: S. Lees and L.A. Ferrari), Plenum Press, New York, **23,** 441-446 (1997).

7   S.A. Nielsen, S.I. Andersen and H. Toftegaard, "An ultrasonic circular aperture technique to predict elastic constants of fiber reinforced composites". In: *Acoustical Imaging* (Ed.: H. Lee), Plenum Press, New York, **24,** 215-222 (1998).

8   S.A. Nielsen and H. Toftegaard, "Ultrasonic measurement of elastic constants in fiber-reinforced polymer composites under influence of absorbed moisture", *Ultrasonics* **38**, 242-246, 2000.

9   R.M. Alford, K.R. Kelly and D.M. Boore, "Accuracy of finite-difference modeling of the acoustic wave equation", *Geophysics* **39**, 834-42 (1974).

10   K.R. Kelly, R.W. Ward, S. Treitel and R.M. Alford, "Synthetic seismograms: a finite difference approach", *Geophysics* **41**, 2-27 (1976).

11   D. Kosloff and E. Baysal, "Forward modeling by the Fourier method", *Geophysics* **47**, 1402-1412 (1982).

12   B. Fornberg, "The pseudospectral method: comparison with finite differences for the elastic wave equation", *Geophysics* **52**, 483-501 (1987).

13   B. Fornberg, "The pseudospectral method: accurate representation of interfaces in elastic wave calculations", *Geophysics* **53**, 625-37 (1988).

14   D. Kosloff, M. Reshef and D. Loewenthal, "Elastic wave calculations by the Fourier method", *Bull. Seism. Soc. Amer.* **74**, 875-91 (1984).

[15] D.C. Witte and P.G. Richards, "The pseudospectral method for simulating wave propagation". In: *Computational Acoustics* (Eds. D. Lee et al.), Elsevier Science Pub., North Holland **3**, 1-18 (1990).

[16] B. Fornberg, *A Practical Guide to Pseudospectral Methods*, Cambridge University Press, Cambridge (1996).

[17] G. Raggio, "A pseudo spectral Chebyshev scheme for forward acoustic modeling", *Z. Angew. Math. Mech.* **66**, 545-553 (1986).

[18] E. Tessmer, D. Kosloff and A. Behle, " Elastic wave propagation simulation in the presence of surface topography, *Geophys. J. Int.* **108**, 621-632 (1992).

[19] D. Kosloff *et al.*, "Solution of the equations of dynamic elasticity by a Chebyshev spectral method", *Geophysics* **55**(6), 734-748 (1990).

[20] E. Tessmer and D. Kosloff, "3-D elastic modeling with surface topography by the Chebyshev spectral method", *Geophysics* **59**, 464-473 (1994).

[21] J.M. Augenbaum, "Multidomain adaptive pseudospectral methods for acoustic wave propagation in discontinuous media". In: *Computational Acoustics* (Eds. D. Lee et al.), Elsevier Science Pub., North Holland **3**, 19-40 (1990).

[22] J.M. Carcione, "Domain decomposition for wave propagation problems", *J. Sci. Comp.* **6**(4), 453-472 (1991).

[23] L. Halpern and L.N. Trefethen, "Wide-angle one-way wave equations", *J. Acoust. Soc. Amer.* **84**, 1397-1404 (1988).

[24] R.L. Higdon, "Radiation boundary conditions for elastic wave propagation", *SIAM J. Numer. Anal.* **27**, 831-870 (1990).

[25] L.T. Long and J.S. Liow, "A transparent boundary for finite-difference wave simulation", *Geophysics* **55**, 201-208 (1990).

[26] J.M. Carcione, "Boundary conditions for wave propagation problems", *Finite Elements in Analysis and Design* **16**, 317-327 (1994).

[27] M.J. Yedlin and Y. Luo, "Incorporation of absorbing boundary conditions into acoustic and elastic wave propagation problems solved by spectral time-marching", *Advances in Engineering Software* **26**, 161-167 (1996).

[28] A. Bayliss and E. Turkel, "Mappings and accuracy for Chebyshev pseudospectral approximations", *J. Comput. Phys.* **101**, 349-359 (1992).

[29] C. Canuto, M.Y. Hussaini, A. Quarteroni and T.A. Zang, *Spectral Methods in fluid dynamics,* Springer-Verlag, New-York (1988).

[30] G.E. Karniadakis and S.J. Sherwin, *Spectral/hp element methods for CFD*. Oxford University Press. Oxford, UK (1999).

[31] P.G. Dinesen, J.S. Hesthaven J.P. Lynov and L. Lading, "Pseudospectral method for the analysis of diffractive optical elements", *J. Opt. Soc. Am.* A/Vol. **16**, 1124-1130 (1999).

[32] J.S. Hesthaven, P.G. Dinesen and J.P. Lynov, "Spectral collocation time-domain modeling of diffractive optical elements", *J. Comput. Phys.* **155**, 287-306 (1999)

[33] D. Gottlieb and S.A. Orszag, "Numerical Analysis of Spectral Methods: Theory and Applications", *SIAM* **26** (1989).

[34] D. Gottlieb and J.S. Hesthaven, " Spectral methods for hyperbolic problems" *J. Comp. Appl. Math.* (2001) (to appear).

[35] J.D. Achenbach, *Wave propagation in elastic solids*, North Holland Publ. Co. (1975).

[36] J. Virieux, "P-SV wave propagation in heterogeneous media: velocity-stress finite-difference method", *Geophysics* **51**, 889-901 (1986).

[37] A. Bayliss, K.E. Jordan, B.J. LeMesurier and E. Turkel, "A fourth-order accurate finite-difference scheme for computation of elastic waves", *Bull. Seismological Soc. Am.* **76**(4), 1115-1132 (1986).

[38] W.J. Gordon and C.H. Hall, "Construction of curvilinear coordinate systems and applications to mesh generation", *Int. Jour. Num. Meth. Eng.* **7**, 461-477 (1973).

[39] W.J. Gordon and C.H. Hall, "Transfinite element methods: blending-function interpolation over arbitrary curved element domains", *Numer. Math.* **21**, 109-129 (1973).

[40] B. Yang, D. Gottlieb, and J.S. Hesthaven, "Spectral simulations of electromagnetic wave scattering", *J. Comput. Phys.* **134**, 216-230 (1997).

TABLE I. Global error of the velocity component v_z for
Lamb's problem as a function the grid points per wavelength.

Parameter	Symbol	Grid Points (N)		
		12 x 12	16 x 16	16 x 16
Grid points /Wavelength	*Nppw*	10.6	14.2	14.2
Step size	*dt*	0.033	0.018	0.0078
Global error	*E*	0.13	0.077	0.077

TABLE II. Material parameters used in the calculation of two-layer simulation.

Parameter	Symbol	Value	
		Steel	Lead
P-wave velocity	C_p (m/s)	5900	2050
S-wave velocity	C_s (m/s)	3200	670
Poisson ratio	v	0.29	0.44
Lamé constant	λ (Gpa)	113.2	16.5
Lamé Constant	μ (Gpa)	80.9	5.5
Mass density	ρ (g/cm^3)	7.9	11.3

Figure Captions

FIG. 1. Mapping between physically curved grid onto auxiliary rectangular grid.

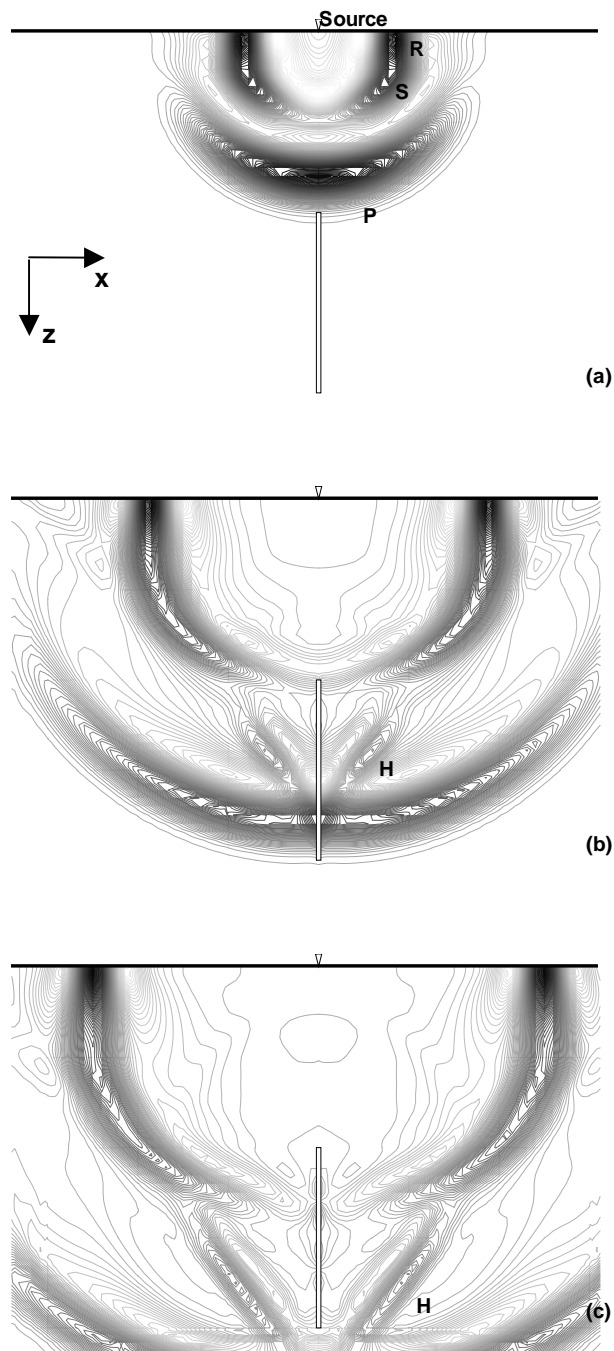FIG. 2. Decomposition of Lamb's problem into 40 subdomains.

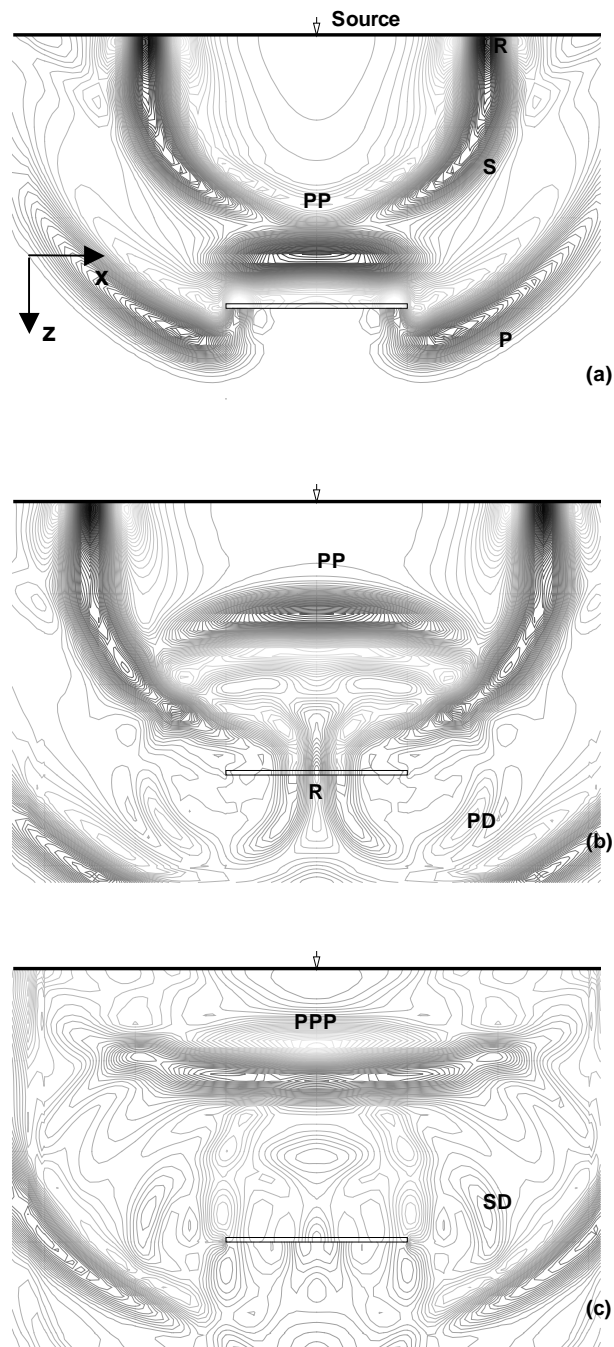FIG. 3. Elastic scattering from a vertical slit due to a point force (a) $t = 1.8$ μs, (b) $t = 4.1$ μs, and (c) $t = 5.5$ μs.

FIG. 4. Elastic scattering from a horizontal slit due to a point force (a) $t = 4.1$ μs, (b) $t = 5.5$ μs, and (c) $t = 8.2$ μs.
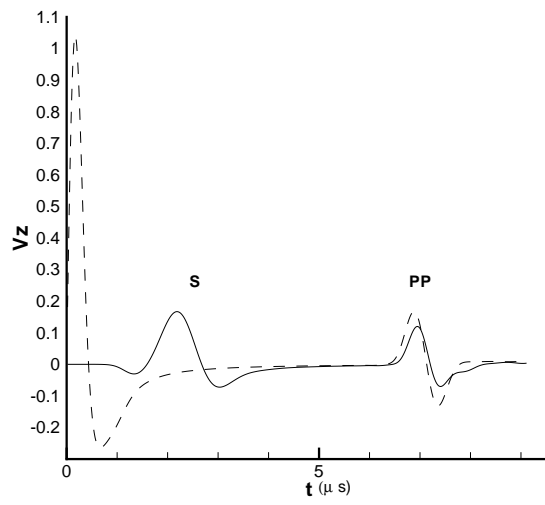
FIG. 5. Time history (A-scan) comparison between elastic v_z component at (x,z)=(0,0) and (0,2).
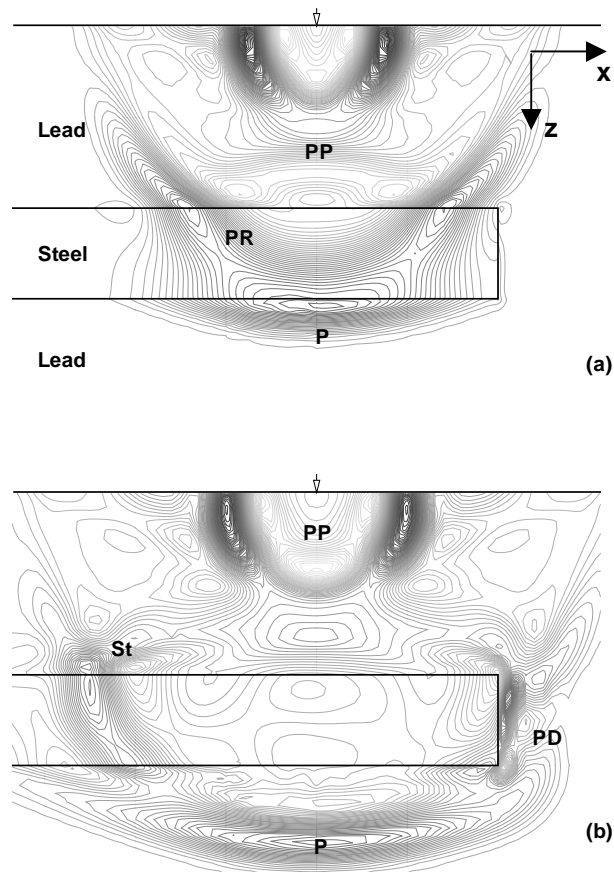
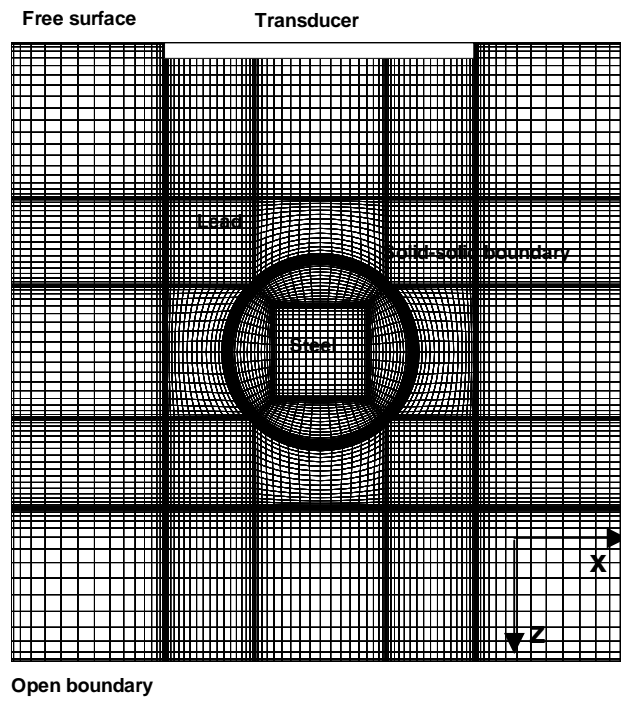FIG. 6. Snapshot of particle velocity in two different elastic solids (a) $t = 7.4$ μs, and (b) $t = 9.8$ μs.

FIG. 7. Decomposition of cylinder into 29 subdomains.

FIG. 8. Scattering from elastic cylinder due to a line source (a) $t = 4.9$ μs, and (b) $t = 7.1$ μs.

FIG. 9. B-scan of backscattered velocity component.

FIG. 1. Mapping between physically curved grid onto auxiliary rectangular grid.
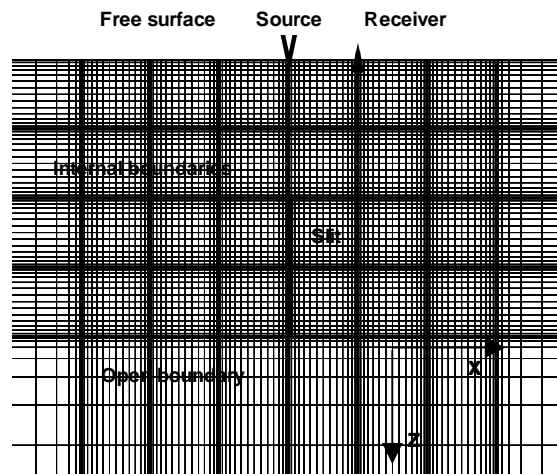
FIG. 2. Decomposition of Lamb's problem into 40 subdomains.

FIG. 3. Elastic scattering from a vertical slit due to a point force
(a) $t = 1.8$ μs, (b) $t = 4.1$ μs, and (c) $t = 5.5$ μs.

FIG. 4. Elastic scattering from a horizontal slit due to a point force
(a) $t = 4.1$ μs, (b) $t = 5.5$ μs, and (c) $t = 8.2$ μs.

FIG. 5. Time history (A-scan) comparison between elastic v_z component at $(x,z)=(0,0)$ and $(0,2)$.

FIG. 6. Snapshot of particle velocity in two different elastic solids.
(a) $t = 7.4\ \mu$s, and (b) $t = 9.8\ \mu$s.
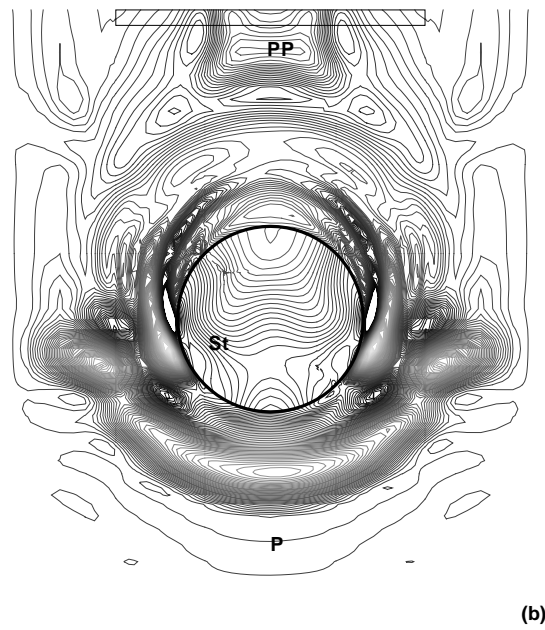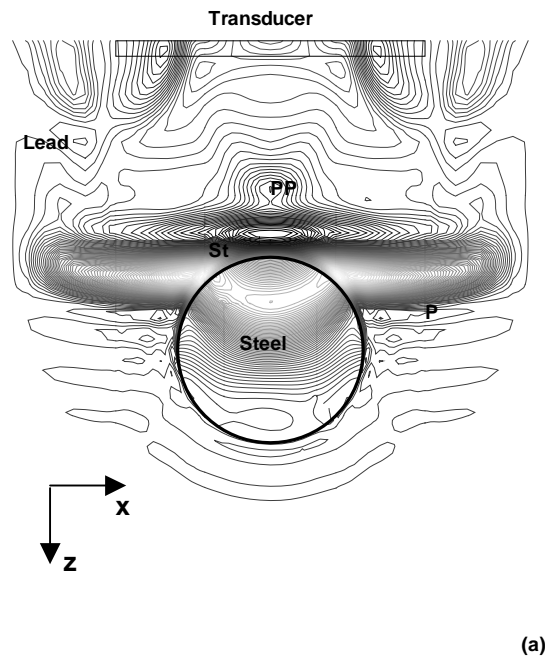
FIG. 7. Decomposition of cylinder into 29 subdomains.

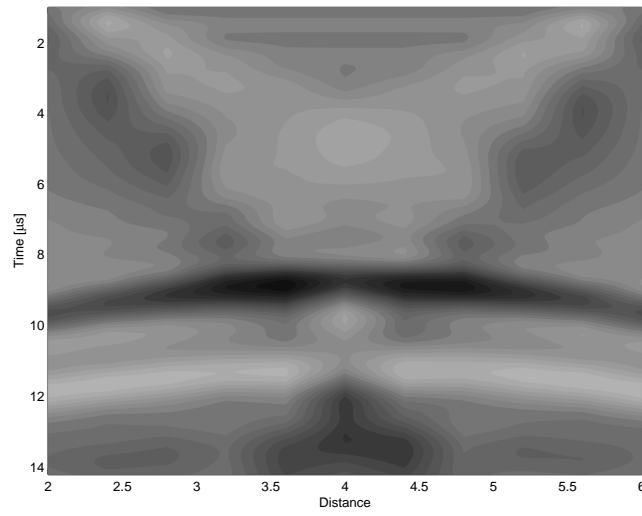FIG. 8. Scattering from elastic cylinder due to a line source.
(a) $t = 4.9$ μs, and (b) $t = 7.1$ μs.

FIG. 9. B-scan of backscattered velocity component.